MYC overexpression leads to increased chromatin interactions at super-enhancers and MYC binding sites

Yi Xiang See,[1,2,3] Kaijing Chen,[1,2,3] and Melissa J. Fullwood[1,2,3,4]

[1] *School of Biological Sciences, Nanyang Technological University, Singapore 637551;* [2] *Cancer Science Institute of Singapore, National University of Singapore, Singapore 117599;* [3] *NUS Centre for Cancer Research, Yong Loo Lin School of Medicine, National University of Singapore, Singapore 117599;* [4] *Institute of Molecular and Cell Biology, Agency for Science, Technology and Research (A*STAR), Singapore 138673*

The *MYC* oncogene encodes for the MYC protein and is frequently dysregulated across multiple cancer cell types, making it an attractive target for cancer therapy. *MYC* overexpression leads to MYC binding at active enhancers, resulting in a global transcriptional amplification of active genes. Because super-enhancers are frequently dysregulated in cancer, we hypothesized that MYC preferentially invades into super-enhancers and alters the cancer genome organization. To that end, we performed ChIP-seq, RNA-seq, circular chromosome conformation capture (4C-seq), and Spike-in Quantitative Hi-C (SIQHiC) on the U2OS osteosarcoma cell line with tetracycline-inducible *MYC*. *MYC* overexpression in U2OS cells modulated histone acetylation and increased MYC binding at super-enhancers. SIQHiC analysis revealed increased global chromatin contact frequency, particularly at chromatin interactions connecting MYC binding sites at promoters and enhancers. Immunofluorescence staining showed that MYC molecules formed punctate foci at these transcriptionally active domains after *MYC* overexpression. These results demonstrate the accumulation of overexpressed MYC at promoter–enhancer hubs and suggest that MYC invades into enhancers through spatial proximity. At the same time, the increased protein–protein interactions may strengthen these chromatin interactions to increase chromatin contact frequency. *CTCF* siRNA knockdown in *MYC*-overexpressed U2OS cells demonstrated that removal of architectural proteins can disperse MYC and abrogate the increase in chromatin contacts. By elucidating the chromatin landscape of MYC-driven cancers, we can potentially target MYC-associated chromatin interactions for cancer therapy.

[Supplemental material is available for this article.]

Dysregulation of the *MYC* oncogene, which encodes for the MYC transcription factor, is common in cancer. Elevated mRNA and protein expression of *MYC* is seen across most cancer types in The Cancer Genome Atlas (TCGA) data set (Schaub et al. 2018), making it an attractive target for cancer therapy. However, there are a multitude of causes for *MYC* dysregulation, including focal amplification of the *MYC* gene (Beroukhim et al. 2010), aberrations in the web of oncogenic signaling pathways regulating *MYC* (Kress et al. 2015), and the acquisition of new enhancer regulatory elements in spatial proximity to the *MYC* gene locus through deletions and translocations (Affer et al. 2014). The MYC protein itself is notoriously termed as "undruggable," because of the unstructured nature of the protein and the lack of enzymatic binding sites or prominent pockets for small molecule inhibitor binding (McKeown and Bradner 2014).

MYC usually binds to the promoters of actively transcribing genes at physiological levels. Upon overexpression, MYC not only increases binding at active promoters but "invades" into active enhancers as well, resulting in a global transcriptional amplification of active genes (Lin et al. 2012). Canonical MYC binding sites become saturated and MYC occupies noncanonical binding sites with lower affinity, resulting in an up-regulation of genes associated with malignant transformation (Walz et al. 2014). Enhancer invasion has also been observed in the MYC family member MYCN (Zeid et al. 2018).

At present, the mechanism underlying MYC enhancer invasion has not been well studied. Enhancers recruit transcription factors to activate linearly distant gene promoters via long-range chromatin interactions (Carter et al. 2002; Plank and Dean 2014). Recent studies have defined a category of enhancers known as super-enhancers: clusters of enhancers with exceptionally high enrichment of transcriptional activators (Hnisz et al. 2013; Lovén et al. 2013; Whyte et al. 2013). Super-enhancers are associated with a more extensive network of chromatin interactions to multiple distant target genes (Cao et al. 2017), to serve as regulatory hubs to govern processes important to cell identity (Whyte et al. 2013). This led us to question whether MYC enhancer invasion might preferentially occur at super-enhancers and if this might alter the cancer genome architecture.

In this study, we aimed to investigate the immediate changes to the enhancer and chromatin interaction landscapes after *MYC* overexpression, particularly at super-enhancers, using Spike-In Quantitative Hi-C (SIQHiC), a modified Hi-C approach that normalizes chromatin interactions by cell count.

Results

MYC overexpression leads to increased MYC binding at super-enhancers

We profiled the MYC enhancer binding landscape changes associated with *MYC* overexpression using the U2OS osteosarcoma cell line

Corresponding author: mfullwood@ntu.edu.sg
Article published online before print. Article, supplemental material, and publication date are at https://www.genome.org/cgi/doi/10.1101/gr.276313.121. Freely available online through the *Genome Research* Open Access option.

inserted with a tetracycline-inducible *MYC* cassette, because these cells are not addicted to *MYC* expression and have been used in previous studies to investigate the effects of *MYC* overexpression (Walz et al. 2014; Lorenzin et al. 2016). Doxycycline treatment for 30 h increased *MYC* gene expression by about 35× compared to vehicle treatment, together with an increase in MYC protein expression (Supplemental Fig. S1A–C). Hereafter, we refer to vehicle-treated and doxycycline-treated U2OS cells as Low *MYC* cells and High *MYC* cells, respectively. RNA-seq identified 548 significantly up-regulated and 842 significantly down-regulated transcripts after *MYC* overexpression (Fig. 1A), in line with previous observations by Walz et al. (2014). MYC is known to repress a subset of genes, for example, through its association with ZBTB17 (also known as MIZ1) (Walz et al. 2014). Although down-regulated transcripts outnumbered up-regulated transcripts (Fig. 1B), only 12.7% of the down-regulated transcripts were direct targets of MYC, indicating that direct repression was not the main mechanism for down-regulation. Most of these down-regulated transcripts were lowly expressed, with reads per kilobase per million (RPKM) values <1. Because *MYC* overexpression had been shown to increase total RNA content per cell (Lovén et al. 2012), transcripts that were up-regulated to a smaller extent than the increase in total RNA content would appear to be down-regulated (Kress et al. 2015). In contrast to the down-regulated transcripts, 24.5% of the up-regulated transcript promoters were bound by MYC at endogenous *MYC* expression levels and increased to 36.9% after *MYC* overexpression (Fig. 1B).

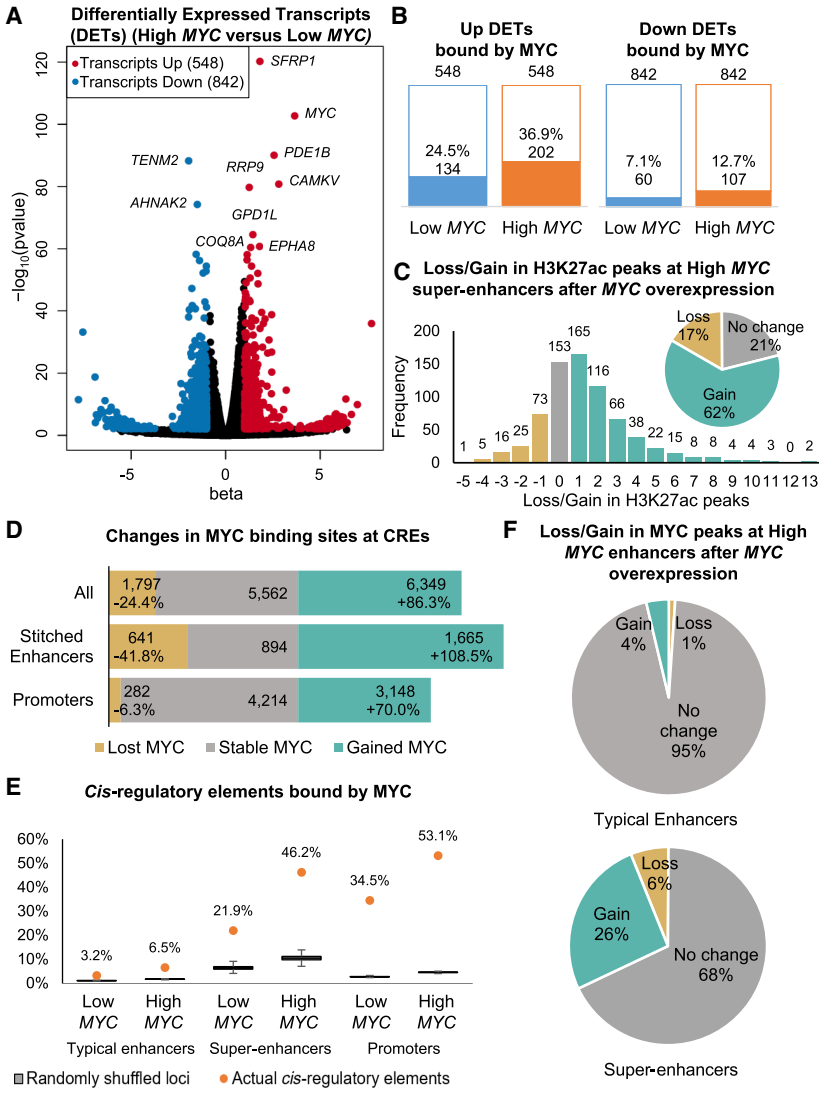

Figure 1. *MYC* overexpression leads to differential transcript expression, differential H3K27ac signal, and increased MYC binding at super-enhancers. (*A*) Significantly up-regulated (red) and down-regulated (blue) transcripts after *MYC* overexpression (|beta| > 1, FDR < 0.05, Wald test). Top 10 significantly regulated transcripts are labeled. (*B*) Number of differentially expressed transcripts (DETs) bound by MYC in Low *MYC* and High *MYC* cells. (*C*) Bar graph and pie chart showing gain and loss of H3K27ac peaks at super-enhancers after *MYC* overexpression. (*D*) Bar graph showing gain and loss of MYC binding sites at stitched enhancers and promoters after *MYC* overexpression. (*E*) Proportion of typical enhancers, super-enhancers, and promoters being bound by MYC compared to randomly shuffled coordinates. The proportion of MYC-bound CREs are shown as orange dots. Box plots show 1000 iterations of MYC occupancy at random genomic loci of the same size and on the same chromosome as the actual CREs. (*F*) Pie charts showing gain and loss of MYC ChIP-seq peaks at typical enhancers (*top*) and super-enhancers (*bottom*) after *MYC* overexpression.

We performed a gene set enrichment analysis (GSEA) to determine the pathways dysregulated by *MYC* overexpression. Previously published gene sets of *MYC*-regulated genes were significantly enriched in our data set (Supplemental Fig. S1D). Consistent with previous literature (Eilers and Eisenman 2008), *MYC* overexpression activated pathways involved in cell proliferation, including ribosome biogenesis, translation, mitochondrial biogenesis, and splicing (Supplemental Fig. S1E). *MYC* overexpression activated the MAPK14 pathway, which is implicated in osteoblast motility (Supplemental Fig. S1E; Rodríguez-Carballo et al. 2016), and down-regulated cell adhesion genes (Supplemental Fig. S1F), suggesting a shift toward a cell migration phenotype.

We performed H3K27ac ChIP-seq to identify active *cis*-regulatory elements (CREs) in Low *MYC* and High *MYC* cells. H3K27ac peaks within 2.5 kb of transcription start sites were labeled as active promoter peaks, whereas the remaining peaks were labeled as enhancer peaks. We identified super-enhancers using a similar approach to ROSE (rank ordering of super-enhancers) (Lovén et al. 2013; Whyte et al. 2013). Briefly, enhancer peaks within 12.5 kb of each other were stitched together, and super-enhancers were separated from typical enhancers based on their H3K27ac ChIP-seq signal (Methods; Supplemental Fig. S2A). In total, we identified ~28,500 stitched enhancers in both Low *MYC* and High *MYC* cells, of which ~7300 stitched enhancers were lost and gained after *MYC*

overexpression (Supplemental Fig. S2C). We identified 890 super-enhancers in the Low *MYC* cells and 725 super-enhancers in the High *MYC* cells (Supplemental Fig. S2E). Although many stitched enhancers were gained or lost, almost all High *MYC* super-enhancers overlapped with Low *MYC* stitched enhancers (Fig. 1C), indicating that super-enhancers remain highly acetylated and novel super-enhancers were not activated after *MYC* overexpression. Sixty-two percent of the High *MYC* super-enhancers gained between 1 and 13 H3K27ac peaks after *MYC* overexpression (Fig. 1C), with 15% merging multiple Low *MYC* stitched enhancers (Supplemental Fig. 2F), resulting in super-enhancers with significantly more constituent H3K27ac peaks (Supplemental Fig. 2G).

Next, we looked into MYC occupancy at CREs. *MYC* overexpression led to a loss of 1797 MYC binding sites and a gain of 6349 MYC binding sites, of which 3148 binding sites were gained at promoters and 1665 at stitched enhancers (Fig. 1D). The proportion of MYC binding sites at stitched enhancers increased from 17.6% to 21.4%, whereas the proportion of MYC binding sites at promoters remained similar (61.5%–61.8%) (Supplemental Fig. 3A), recapitulating previous observations of enhancer invasion. The 21.9% of super-enhancers overlapping with MYC binding sites increased to 46.2% after *MYC* overexpression (Fig. 1E). and 26% of super-enhancers gained MYC binding sites after *MYC* overexpression, compared to only 4% of typical enhancers (Fig. 1F; Supplemental Fig. S3B,C). H3K27ac ChIP-seq profiles of MYC binding sites show that MYC binds directly adjacent to constituent H3K27ac peaks and not randomly between the constituent peaks within the super-enhancers (Supplemental Fig. S3D). To test whether the preferential binding of MYC at super-enhancers was due to size, we randomly shuffled the genomic intervals of CREs within the same chromosome and overlapped them with MYC binding sites. Significantly more actual super-enhancers overlapped with MYC binding sites than 1000 iterations of randomly shuffled genomic loci (Fig. 1E), indicating that MYC preferentially binds at super-enhancers regardless of their size. Together, these results indicate that overexpressed MYC preferentially accumulates at H3K27ac peaks in super-enhancers.

We further compared the MYC binding sites that were pre-existing, lost, or gained after *MYC* overexpression. Pre-existing MYC binding sites at promoters and enhancers consistently had the highest H3K27ac and MYC ChIP-seq signals, whereas gained MYC binding sites had lower signals (Supplemental Fig. S3E–G), indicating that open chromatin demarcated by H3K27ac is required for MYC binding. Lost promoter MYC binding sites had high H3K27ac signal comparable to pre-existing and gained MYC binding sites (Supplemental Fig. S3G). This suggests that H3K27ac is required but insufficient for MYC binding at promoters, and other factors are involved in the recruitment of MYC, such as binding site affinity and recruitment by other transcription factors (Lorenzin et al. 2016).

We performed motif analysis at MYC ChIP-seq peaks to ascertain whether there may be different chromatin factors recruiting MYC to promoters and enhancers. Promoter MYC binding sites were more enriched for other transcription factor binding motifs compared to typical enhancer and super-enhancer MYC binding sites (Supplemental Fig. S4A,B). Thirty-five motifs occurred at >50% of promoter MYC binding sites, whereas no single motif occurred at >50% of enhancer MYC binding sites (Supplemental Fig. S4A,B). Top enriched motifs at promoters included known promoter binding factors such as the KLF/SP family of transcription factors, which contain guanine/cytosine (G/C) rich sequences. Similarly, top enriched motifs at enhancers contained G/C rich sequences, such as MAZ, ZBTB17, and EGR2. Chromatin interactions frequently connect CpG rich promoters and enhancers together (Pachano et al. 2021), and these interactions may be mediating the recruitment of MYC from promoter binding sites to enhancers. Gained MYC binding sites were slightly less enriched for transcription factor motifs than pre-existing MYC binding sites (Supplemental Fig. S4F), whereas lost MYC binding sites were poorly enriched for transcription factor motifs, suggesting that MYC is likely recruited to these binding sites by other transcription factors (Supplemental Fig. S4G). However, the same transcription factor motifs were enriched for in lost, pre-existing, and gained MYC binding sites, indicating that recruitment of supraphysiological MYC to gained binding sites by new interactors is unlikely (Supplemental Fig. S4E).

Spike-in Quantitative Hi-C reveals increased global chromatin contact frequency per cell after *MYC* overexpression

In traditional Hi-C techniques, cross-sample normalization is based on the assumption that chromatin interactions are largely stable across biological conditions (Lun and Smyth 2015; Stansfield et al. 2018). However, perturbation of factors involved in chromatin organization such as CTCF and cohesin can result in global changes in chromatin contact frequency. We hypothesized that increased global MYC binding at CREs not only increases transcription of associated genes but also stabilizes chromatin interactions at these genes, resulting in similar global changes in chromatin contact frequency.

Cell-count normalization techniques have been developed for RNA-seq (Lovén et al. 2012) and ChIP-seq (Orlando et al. 2014) to account for global changes in transcription and occupancy, respectively. Cell-count normalized transcription analyses had previously revealed a global increase in transcription after *MYC* overexpression (Lovén et al. 2012; Nie et al. 2012). These methods involve mixing a control sample from an orthogonal species into the experimental human samples at a fixed cell number ratio. The recently published Absolute Quantification of Architecture Hi-ChIP protocol (AQuA-HiChIP) (Gryder et al. 2019) utilizes the same strategy of spiking in mouse cells into human samples, running on the assumption that contact frequency for untreated mouse cells should be the same across samples.

In our study, we adapted the AQuA-HiChIP protocol (Gryder et al. 2019) to perform Spike-In Quantitative Hi-C on Low *MYC* and High *MYC* cells in duplicate, to elucidate the global changes in chromatin contact frequency. In brief, mouse 3T3 cells were cross-linked and mixed into each sample of human cells at a ratio of 1:4, before continuing with the Arima Hi-C kit protocol (Fig. 2A; Methods), preserving this cell number ratio throughout all subsequent steps of library preparation. If global chromatin contact frequency is unchanged, we expect to obtain a similar human to mouse chromatin contact ratio (HMR) across all samples. Hence, the relative difference between the HMR of different samples reflects the differences in global chromatin contact frequency and can be used to normalize the samples (Fig. 2B).

Ambiguous read pairs mapping to both species consistently made up a small percentage of the total reads per sample (~0.3%) and were discarded (Supplemental Table S1). Using SIQHiC, we observe a 2.1- to 4.4-fold increase in HMR after *MYC* overexpression, suggesting an equivalent increase in global chromatin contacts (Supplemental Table S2). Hi-C chromatin interaction heat maps of Low *MYC* and High *MYC* cells appear to show a decrease in chromatin interactions after *MYC* overexpression (Fig. 2C, left). After

SIQHiC normalization, we observed an increase in chromatin interactions instead (Fig. 2D, right). As expected, Low *MYC* duplicates had similar HMRs (33.4 and 36.4), reflecting consistent chromatin contact frequencies at physiological *MYC* levels (Supplemental Table S2). Conversely, High *MYC* duplicates had higher and more variable HMRs (146.9 and 78.1) after doxycycline induction of *MYC* expression. (Supplemental Table S2).

MYC overexpression weakens TAD insulation and strengthens a set of chromatin loops

Given that *MYC* overexpression increased chromatin contact frequency, we wanted to know whether *MYC* overexpression reshapes the global chromatin landscape. A/B compartment analysis showed few instances of compartment switching between Low *MYC* and High *MYC* cells, with Chromosome 8 shown as an example in Supplemental Figure S5A. However, *MYC* overexpression weakened insulation at topologically associating domain (TAD) boundaries (Supplemental Fig. S5B), resulting in a loss of 2912 TAD boundaries (Supplemental Fig. S5C). Lost and common TAD boundaries showed similar loss of insulation, as seen by the reduced amplitude of TAD separation score, whereas insulation at gained boundaries remained relatively unchanged (Supplemental Fig. S5B). This indicates that inactive compartments were not activated by *MYC* overexpression, but chromatin contact frequency increased interactions across TAD boundaries.

Next, we identified 7266 and 7910 significant chromatin loops in Low *MYC* and High *MYC* cells, respectively, with approximately 60% of these loops common between both conditions (Supplemental Fig. S5D). We performed an aggregate plot analysis (APA) to show the aggregate signal of the chromatin loops that were "gained" and "lost" after *MYC* overexpression, or "common" between both conditions. In this analysis, the 105-kb × 105-kb contact matrices surrounding the midpoints of all loops in each loop set are overlapped such that the center pixel (P) of the APA plot shows the aggregate signal of the midpoints of these loops. The lower left corner of the plot (LL) represents the contact frequency for shorter interactions in the vicinity of the loop set and gives an indication of the local random interaction frequencies. Without SIQHiC normalization, APA plots show decreased peak signal enrichment (P) at chromatin loops after *MYC* overexpression (Supplemental Fig. S6A,B). Using SIQHiC to normalize for cell count revealed a 2.2- and 3.3-fold increase in peak signal enrichment (P) at common and gained loop sets instead (Supplemental Fig. S6C,D). Using the ratio of signal at P to the average signal at LL (P2LL) to normalize peak signals against local background interactions, we observed a smaller increase in chromatin contact frequency at common and gained loop sets compared to SIQHiC normalization (1.4-fold and 2.1-fold, respectively) (Fig. 2D,E), indicating that *MYC* overexpression increased local random interactions but to a lesser extent than loop interactions. Taken together, APA analysis showed that *MYC* overexpression increased global chromatin contact

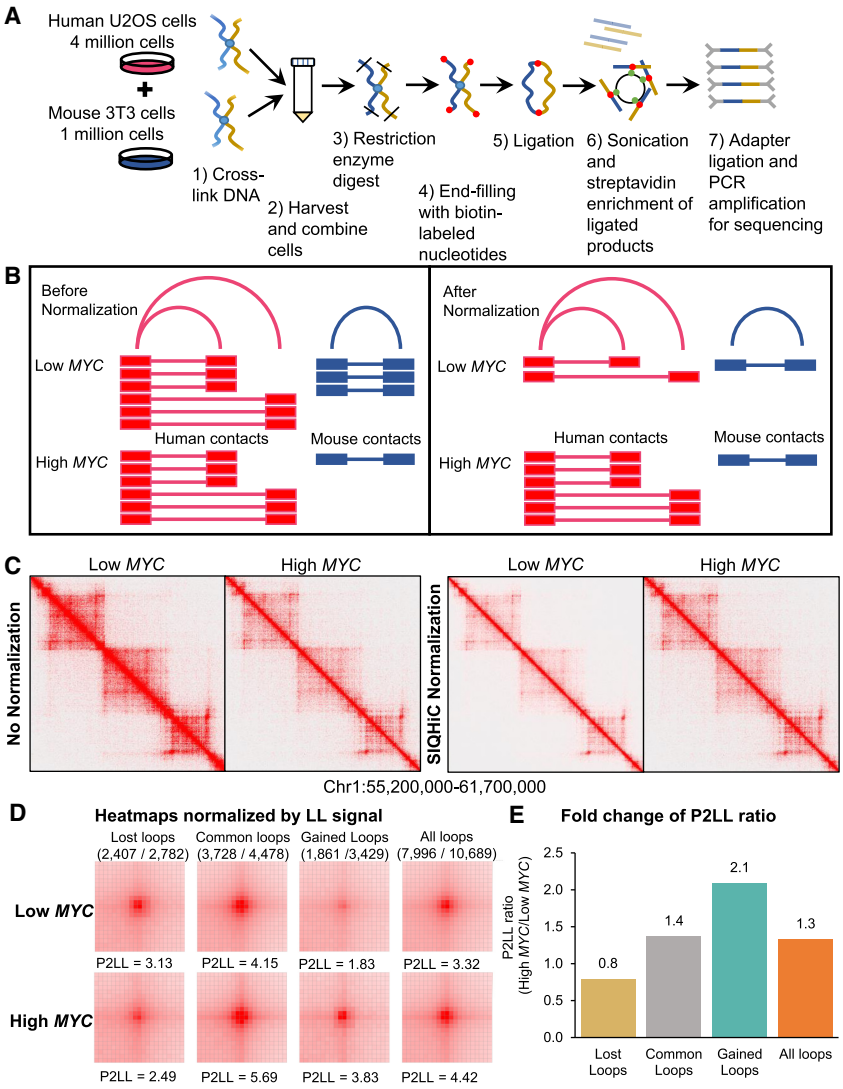

Figure 2. SIQHiC normalization reveals increased chromatin contact frequency per cell after *MYC* overexpression. (*A*) Brief overview of the SIQHiC workflow. (*B*) Cartoon illustrating Hi-C contacts before (*left*) and after (*right*) SIQHiC normalization. SIQHiC normalization scaled down the Low *MYC* contacts such that the number of mouse contacts in both conditions was the same, thereby revealing an increase in human chromatin contacts. (*C*) Hi-C matrix heat maps of a region on Chromosome 1. *Left* panel: No normalization. *Right* panel: SIQHiC normalization. (*D*) Aggregate Peak Analysis (APA) plots at 5-kb resolution showing the aggregate signal of "Lost," "Common," and "Gained" chromatin loop sets in Low *MYC* and High *MYC* cells identified using the nonnormalized Hi-C contact matrices. (P) Peak signal at the center pixel, (LL) average signal of the 3 × 3 square at the *lower left* corner of the APA plot, representing local background, (P2LL) ratio of P to LL. APA color scales were normalized by the LL signal. Loop sets were filtered to remove short loops near the diagonal (shown *above* each APA plot; numerator: number of filtered loops; denominator: total number of loops). (*E*) Fold change of P2LL ratio between High *MYC* and Low *MYC* cells.

frequency as a whole but strengthened these chromatin loops in particular.

We zoomed in on the *MYC* gene locus because *MYC* is known to be regulated by super-enhancers through chromatin interactions (Shi et al. 2013; Herranz et al. 2014; Zhang et al. 2016; Bahr et al. 2018). We generated virtual 4C plots from our Hi-C data, using the *MYC* gene promoter as the viewpoint, to visualize the chromatin interactions at this locus. Without normalization, virtual 4C showed a general decrease in chromatin interaction frequencies (Fig. 3A). However, SIQHiC normalization of the Hi-C reads revealed a general increase in virtual 4C signal instead (Fig. 3A).

Because Hi-C assays the entire genome, it requires very high sequencing depth for sufficient resolution and limits chromatin loop detection within a specific region of interest (Babu and Fullwood 2015; Sati and Cavalli 2017). Hence, we performed circular chromosome conformation capture (4C-seq) at a randomly selected MYC bound super-enhancer near the *PROC* gene which gained a chromatin loop to the *CYP27C1* gene after *MYC* overexpression. 4C-seq showed that the gained Hi-C chromatin loop was already present in Low *MYC* cells, but *MYC* overexpression increased the interaction frequency of this loop (Fig. 3B). 4C-seq also identified additional chromatin loops at the MYC-bound super-enhancer locus that were not significant in the Hi-C data (Fig. 3B, blue arrows). Taken together, *MYC* overexpression strengthens a set of gained chromatin loops.

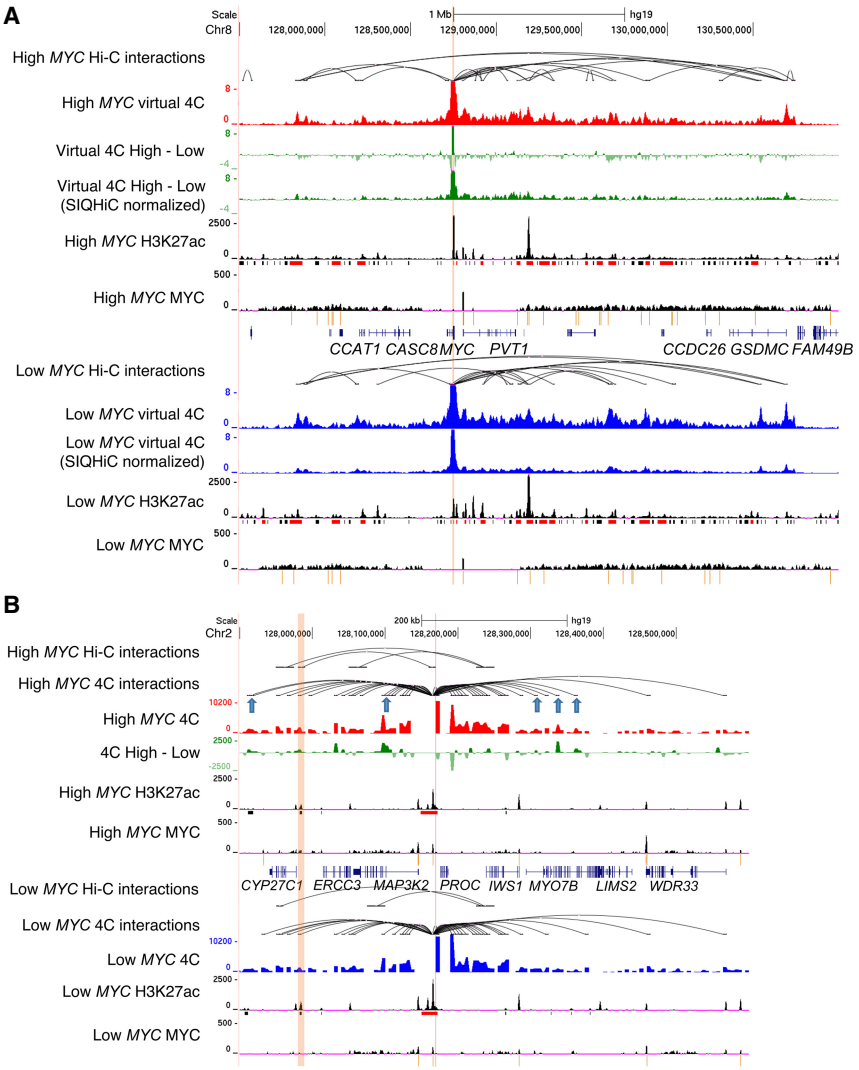

Figure 3. *MYC* overexpression increases chromatin contact frequency and chromatin loops at super-enhancers. (*A*) Genome browser view of High *MYC* and Low *MYC* cells at the *MYC* locus. Tracks show Hi-C chromatin loops, virtual 4C signal of interactions at the *MYC* promoter (red and blue tracks, respectively), H3K27ac and MYC ChIP-seq signal. The difference between the virtual 4C signals of High *MYC* and Low *MYC* cells are shown with and without SIQHiC normalization (green tracks). Super-enhancers (red) and typical enhancers (black) are shown as bars *below* the H3K27ac ChIP-seq tracks. MYC binding peaks are shown as yellow bars *below* the MYC ChIP-seq tracks. (*B*) 4C-seq of chromatin interactions at a randomly selected MYC-bound super-enhancer near the *PROC* gene on Chromosome 2. Tracks show Hi-C chromatin loops, 4C-seq signal (red and blue tracks), difference between 4C-seq signal of High *MYC* and Low *MYC* cells (green), H3K27ac and MYC ChIP-seq signal. Gained Hi-C chromatin loop is highlighted in orange. Blue arrows show additional gained chromatin interactions identified using 4C-seq.

SIQHiC normalization shows reduced chromatin contact frequency after *CTCF* siRNA knockdown

To validate our SIQHiC normalization approach, we transfected High *MYC* cells with either small interfering RNA (siRNA) targeting *CTCF* (siCTCF) or nontargeting siRNA (siControl) and performed SIQHiC in duplicate. siCTCF knockdown reduced *CTCF* expression by 80% compared to siControl (Supplemental Fig. S7A). SIQHiC normalization showed that global chromatin contact frequency in siCTCF cells was reduced by 55% compared to siControl cells (Supplemental Tables S3, S4). After *CTCF* siRNA knockdown, 74.3% (4633/6236) of TAD boundaries from siControl cells remained (Supplemental Fig. S7B), but 47.1% (5624/11,929) of chromatin loops were lost (Supplemental Fig. S7C). TAD boundaries lost after *CTCF* siRNA knockdown showed a decrease in insulation, but insulation at the common and gained TAD boundaries remained mostly unchanged (Supplemental Fig. S7D). These results are similar to previous reports of insulation preservation at selected TAD boundaries when CTCF is incompletely depleted (Zuin et al. 2014; Khoury et al. 2020). Without normalization, siCTCF appeared to selectively decrease chromatin contact frequency at siControl-unique chromatin loops and increase chromatin contact frequency at a small set of siCTCF-unique loops, whereas contact frequency at common loops remained unchanged (Supplemental Fig. S7C,E,F), similar to results from Zuin et al. (2014) and Kubo et al. (2021). After applying SIQHiC normalization, we observed a global decrease in chromatin contact frequency at all loop sets instead (Supplemental Fig. S7G,H),

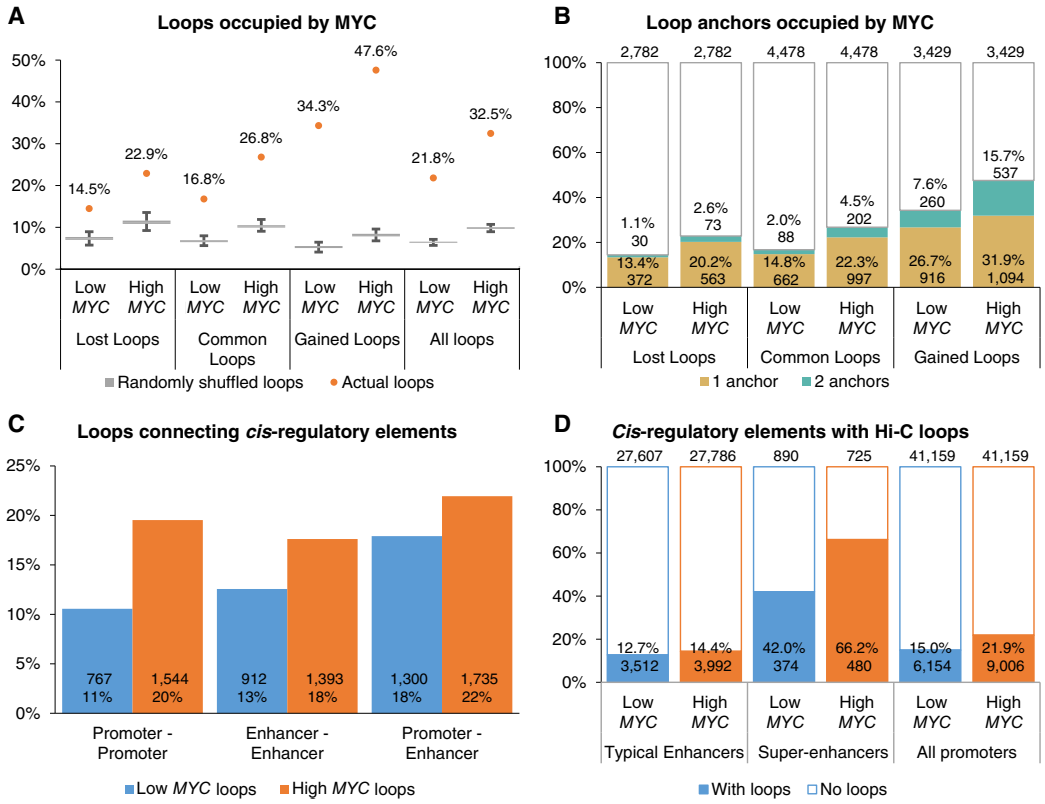

Figure 4. Chromatin interactions are enriched at super-enhancers and gained chromatin loops tend to connect MYC binding sites. (*A*) Percentage of Hi-C chromatin loops occupied by MYC compared to randomly shuffled loop coordinates. Percentage of MYC-bound chromatin loops are shown as orange dots. Box plots show 1000 iterations of MYC occupancy at random genomic loci of the same size and on the same chromosome as the actual chromatin loops. (*B*) Percentage of chromatin loop anchors occupied by MYC. (*C*) Percentage of Hi-C chromatin loops connecting *cis*-regulatory elements. (*D*) Percentage of *cis*-regulatory elements with Hi-C chromatin loops.

indicating that the siCTCF unique loops were not being induced after CTCF depletion but rather reduced to a lesser extent compared to siControl unique and common loops. This demonstrates the necessity for cell-count normalization when perturbing chromatin architectural factors.

Chromatin loops tend to connect MYC binding sites at super-enhancers

We overlapped all Hi-C loop anchors with MYC binding sites and found that the proportion of all chromatin loops with MYC binding sites increased from 21.8% to 32.5% after *MYC* overexpression (Fig. 4A). Gained loops were particularly enriched in MYC binding, with 47.6% of these loops occupied by MYC in High *MYC* cells, which was considerably higher than the proportion of randomly shuffled chromatin loop coordinates overlapping with MYC binding sites (Fig. 4A). Notably, more gained loops were occupied by MYC at physiological MYC levels (34.3%) compared to common (16.8%) and lost loops (14.3%) (Fig. 4A). Additionally, 7.6% of the gained loops had MYC binding at both anchors at physiological MYC levels and increased to 15.7% after *MYC* overexpression (Fig. 4B). APA analysis revealed a 1.54-fold increase in chromatin contact frequency at loops connecting MYC binding sites, compared to a 1.32-fold increase at loops with no MYC binding (Supplemental Fig. S8A). Gene Ontology analysis showed that MYC-bound genes at lost chromatin loops were associated with negative regulation of transcription (Supplemental Fig. S8B). MYC-bound genes at gained chromatin loops were associated with previously shown *MYC* dysregulated pathways such as transcription, translation, and cell–cell adhesion (Supplemental Figs. S1E,F, S8C). These results suggest that chromatin interactions connecting MYC-bound genomic loci are preferentially strengthened after *MYC* overexpression.

Next, we wanted to know whether chromatin interactions are preferentially altered at the enhancers invaded by MYC. We annotated the Hi-C loops according to their overlap with promoters and stitched enhancers. *MYC* overexpression increased chromatin looping between promoters (11%–20%), between stitched enhancers (13%–18%), and between promoters and stitched enhancers (18%–22%) (Fig. 4C). In particular, the proportion of CRE loops within the lost loop set was similar to the common loop set, whereas the proportion of CRE loops within the gained loop set was markedly higher (Supplemental Fig. S9A), showing that chromatin interactions are preferentially strengthened between CREs. Consistent with previous research (Cao et al. 2017), a markedly higher proportion of super-enhancers (42.0%) was associated with Hi-C loops compared to typical enhancers (12.7%) and promoters (15.0%), and *MYC* overexpression further increased the proportion of super-enhancers with loops to 66.2% (Fig. 4D). MYC-bound CREs were more associated with chromatin loops compared to non-MYC-bound CREs, particularly after *MYC* overexpression (Supplemental Fig. S9B). Because super-enhancers are larger than typical enhancers, we compared the constituent H3K27ac peaks within typical and super-enhancers. Similarly, more MYC-bound super-

enhancer constituent H3K27ac peaks overlapped with Hi-C loops (27.3%–39.9%) compared to MYC-bound typical enhancer constituents (13.2%–21.2%) and promoter loci (15.4%–28.0%) (Supplemental Fig. S9B,C).

Because MYC binds at both promoters and enhancers, we looked at promoter–enhancer chromatin loops (P-E loops) in detail. We overlapped P-E loops with MYC binding sites and categorized the loops as being bound proximal to the promoter loop anchor or bound at both loop anchors (Fig. 5A). *MYC* overexpression increased the proportion of P-E loops with only proximal MYC binding sites from 16% to 26%, whereas P-E loops bound at both anchors increased from 3% to 16% (Supplemental Fig. S9D). Although lost P-E loops gained MYC binding sites at the promoter proximal loop anchor after *MYC* overexpression (22%–36%), few of these loci gained MYC at the distal anchor as well (3%–8%) (Fig. 5B). In contrast, gained P-E loops acquired more distal MYC binding sites (9%–23%) (Fig. 5B). Taken together, our results suggest that *MYC* overexpression preferentially strengthens chromatin interactions between MYC binding sites at promoters and enhancers.

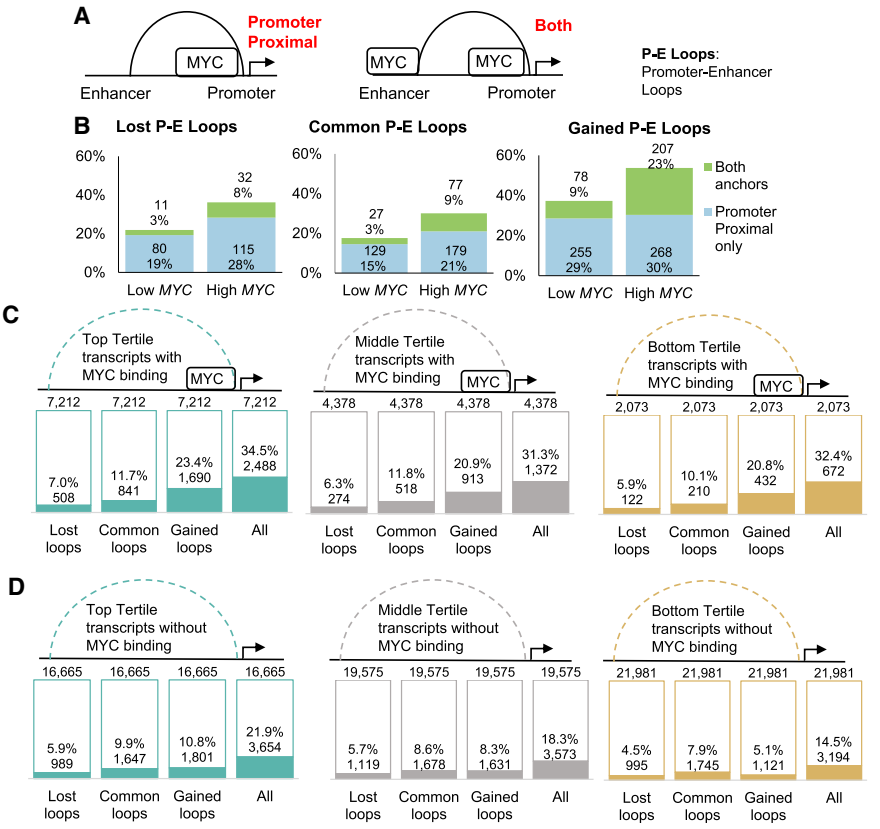

Figure 5. MYC is enriched at both anchors of gained promoter–enhancer chromatin loops regardless of transcriptional activity. (*A*) Promoter–enhancer chromatin loops are categorized as having promoter-proximal MYC binding or MYC binding at both loop anchors. (*B*) Percentage of lost (*left*), common (*middle*), and gained (*right*) promoter–enhancer chromatin loops occupied by MYC at the promoter proximal anchor or at both anchors. (*C*,*D*) Percentage of (*C*) MYC-bound and (*D*) non-MYC-bound transcripts with Hi-C chromatin loops. Transcripts were stratified into top (green), middle (gray), and bottom (yellow) tertiles based on transcript expression after *MYC* overexpression.

MYC overexpression increases chromatin contact frequency regardless of transcription activity

Previous studies have linked transcription activity with the formation of chromatin interactions, possibly through cohesin binding and positioning (Busslinger et al. 2017; Isoda et al. 2017; Heinz et al. 2018) and *cis*-regulatory element mobility (Gu et al. 2018; Nagashima et al. 2019). Because *MYC* overexpression leads to a global increase in transcription, we wanted to know whether the observed increase in chromatin interactions is a result of this increase in transcriptional activity. First, we compared significantly up- and down-regulated transcripts ($P < 0.05$, abs(beta) > 1) with nonregulated transcripts ($P > 0.95$, transcripts per million > 1). Hi-C loops are not preferentially gained or lost at *MYC* regulated transcripts compared to *MYC* nonregulated transcripts (Supplemental Fig. S10A). However, more MYC-bound transcripts gained Hi-C loops (Supplemental Fig. S10B) compared to transcripts without MYC binding (Supplemental Fig. S10C), indicating that MYC binding contributed to chromatin looping regardless of differential transcript expression.

When transcripts were stratified into tertiles based on transcript expression, top tertile transcript promoters overlapped better with Hi-C loops compared to the bottom tertile (25.7% and 16.1%, respectively), demonstrating that transcriptional activity positively correlates with chromatin looping (Supplemental Fig. S11A). However, we found that MYC-bound transcripts were more associated with gained Hi-C loops compared to transcripts without MYC, regardless of expression levels (Fig. 5C,D). Transcripts with pre-existing or gained MYC binding after *MYC* overexpression were more associated with gained Hi-C loops regardless of expression levels (Supplemental Fig. S11B,C), indicating that the direct binding of MYC increases chromatin contact frequency regardless of the level of transcriptional activity.

In contrast, among transcripts that lost MYC binding after *MYC* overexpression, bottom and middle tertile transcripts more associated with lost Hi-C loops and less associated with gained Hi-C loops, whereas top tertile transcripts were associated with gained Hi-C loops (Supplemental Fig. S11D), demonstrating the contribution of transcriptional activity to chromatin contact frequency when MYC is not present. Together, these results show that transcriptional activity correlates with chromatin interactions but the direct binding of MYC also increases chromatin contact frequency through other mechanisms.

Chromatin contacts can be disrupted by removing CTCF

Because chromatin interactions were connecting MYC binding sites together at these regions of high transcriptional activity, we wanted to know whether the overexpressed MYC was being spatially constrained at these regions or merely diffused throughout the nucleus. Immunofluorescence staining showed that MYC formed discrete punctate spots within the nucleus after *MYC*

overexpression, overlapping regions with high RNA polymerase II signal (Supplemental Fig. S12). These punctate spots were lost after *CTCF* siRNA knockdown, indicating that these foci can be disrupted by removing chromatin architectural factors (Supplemental Fig. S12).

To confirm this, we looked at the siCTCF-mediated changes in chromatin interaction frequencies at the common and gained loops after *MYC* overexpression. SIQHiC-normalized APA analysis showed similar reductions in chromatin contact frequency at common and gained loops, which was not evident in the nonnormalized APA plots (Fig. 6A–D). SIQHiC-normalized virtual 4C plots of interactions at the *MYC* promoter illustrated the decrease in chromatin contact frequency (Fig. 6E), recapitulating previous observations in CTCF-depleted SEM cells (Hyle et al. 2019). Although CTCF depletion reduced *MYC* expression in SEM cells (Hyle et al. 2019), *MYC* was not down-regulated in siCTCF cells because of exogenous *MYC* expression from the tetracycline-inducible system (Supplemental Fig. S7A). While maintaining high *MYC* expression, we show that reduction of chromatin architectural proteins such as CTCF can reduce chromatin interactions at MYC foci and disperse MYC. Taken together, we propose a model where MYC accumulates at canonical promoter binding sites, binds to noncanonical binding sites at spatially adjacent super-enhancers, and forms protein–protein interactions with other transcription factors to stabilize chromatin interactions at these domains (Fig. 6F).

Discussion

MYC overexpression has long been described as a key driving force for oncogenesis in multiple cell types, resulting in tumors that become highly dependent on elevated *MYC* expression (Gabay et al. 2014; Bradner et al. 2017), but it is still unclear how overexpressed MYC shifts from regulating its canonical target genes to activate oncogenes. Recent studies have shown that overexpressed MYC invades into distal enhancer regulatory elements to differentially regulate gene expression (Lin et al. 2012; Nie et al. 2012; Sabò et al. 2014). Because cancer cells frequently acquire novel, cancer-specific super-enhancer signatures that are associated with cancer initiation and maintenance (Ooi et al. 2016; Tsang

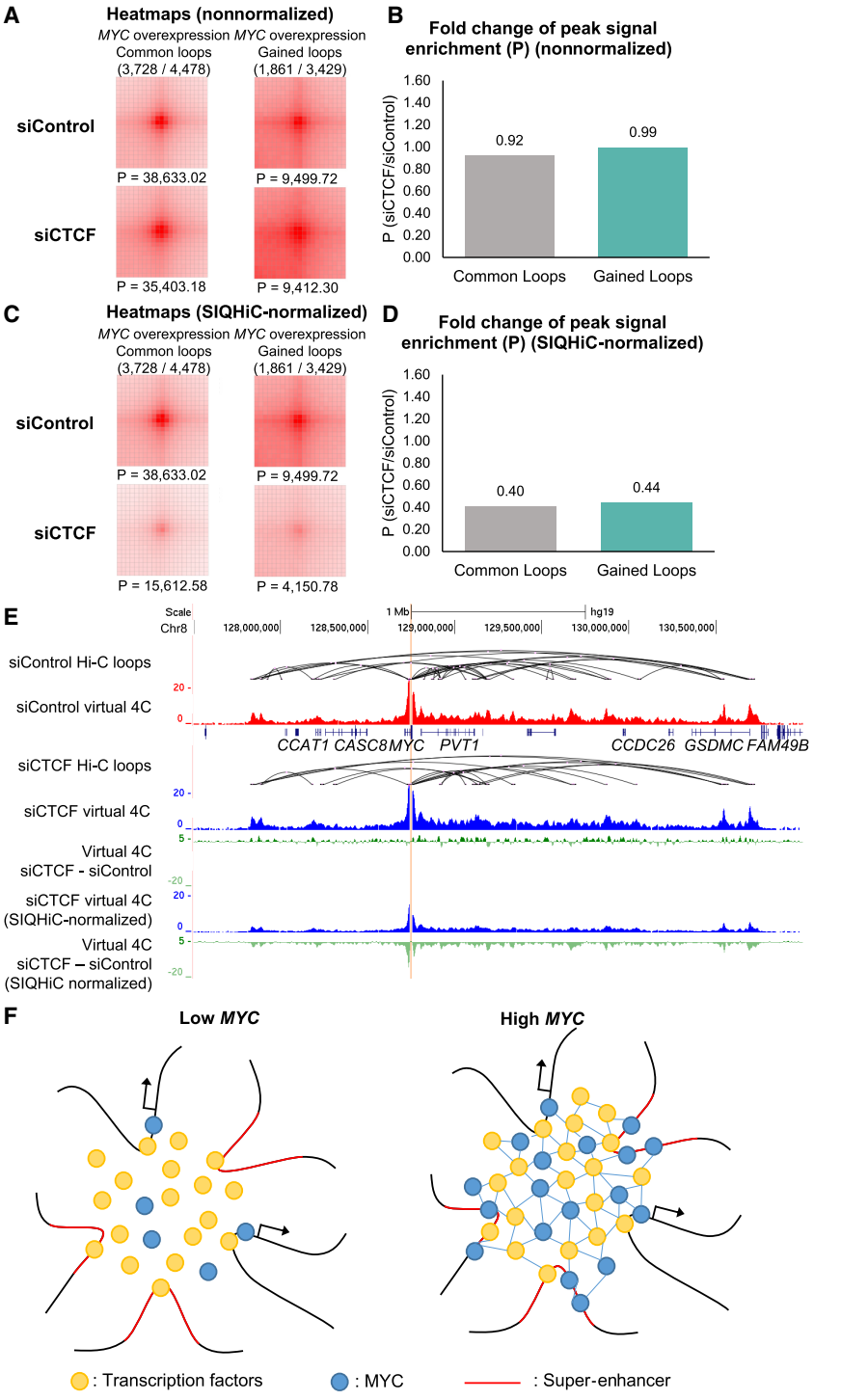

Figure 6. Chromatin contacts can be disrupted through *CTCF* siRNA knockdown. (*A*) siControl and siCTCF Aggregate Peak Analysis plots at 5-kb resolution showing the nonnormalized aggregate signal at "Common" and "Gained" chromatin loops previously identified in High *MYC* cells. (P) Peak signal at the center pixel. (*B*) Fold change of nonnormalized peak signal enrichment (P) at common and gained loops between siControl and siCTCF cells. (*C*) Same APA analysis as in *A* but with SIQHiC normalization applied. (*D*) Fold change of SIQHiC-normalized peak signal enrichment (P) at common and gained loops between siControl and siCTCF cells. (*E*) Genome browser view showing siControl and siCTCF virtual 4C signal of interactions at the *MYC* promoter (red and blue tracks, respectively). The difference between the siControl and siCTCF virtual 4C signals are shown with and without SIQHiC normalization (green tracks). (*F*) Proposed model of overexpressed MYC accumulating at canonical promoter binding sites, binding to spatially adjacent super-enhancers, and forming protein–protein interactions with other transcription factors to stabilize chromatin interactions within the domain.

et al. 2019; Raisner et al. 2020), we wondered whether MYC binds preferentially to super-enhancers to perform its oncogenic functions. In this paper, we use the U2OS cell line with a tetracycline-inducible MYC system, which has been widely used for the study of transcriptional regulation by MYC (Walz et al. 2014; Lorenzin et al. 2016; de Pretis et al. 2017; Nie et al. 2020) and is a reasonable model for establishing a parsimonious understanding of MYC enhancer invasion. We show that overexpressed MYC indeed invades into super-enhancers in particular and leads to changes in the enhancer landscape and chromatin interactome. In particular, super-enhancers gained more constituent H3K27ac peaks and increased enrichment of MYC binding after *MYC* overexpression.

Although there was a loss and gain of more than 7000 stitched enhancers after *MYC* overexpression, we observed no de novo super-enhancer formation at H3K27ac unmarked loci. This is consistent with results from Poli et al. (2018) using TERT-immortalized human mammary epithelial (IMEC) cells, where cancer-associated de novo enhancers were not activated in *MYC*-overexpressed IMEC cells but marked by H3K27ac only after deriving secondary mammospheres. Earlier studies have shown that MYC does not bind to closed chromatin (Guccione et al. 2006; Lin et al. 2012; Soufi et al. 2012), suggesting that MYC invades into active super-enhancers but is unable to activate silent oncogenic super-enhancers by itself.

Because super-enhancers are associated with abundant long-range chromatin interactions and high interaction frequencies (Schmitt et al. 2016; Beagrie et al. 2017; Cao et al. 2017), we wanted to know whether MYC super-enhancer invasion alters the three-dimensional chromatin interactome. Using SIQHiC, a modified Hi-C protocol normalizing for cell count between samples, we observed increased global chromatin contact frequency after *MYC* overexpression. Chromatin interactions at MYC binding sites were preferentially strengthened and connected MYC binding sites together, notably between promoters and enhancers. Kieffer-Kwon et al. (2017) previously showed that *MYC* up-regulation during B cell activation is accompanied by a twofold increase in chromatin loops, particularly the formation of B cell-associated chromatin loops. In this work, *MYC* overexpression alone strengthened pre-existing loops but did not increase the total number of chromatin loops, suggesting that other chromatin factors are required to reconfigure the chromatin interaction landscape in cancer as well as in B cell activation.

Previous studies have shown that *CTCF* siRNA knockdown does not deplete CTCF protein completely and leads to limited disruption of TAD boundaries (Zuin et al. 2014; Khoury et al. 2020), and this was recapitulated in our study. In contrast, degron-mediated CTCF protein degradation resulted in widescale weakening of TAD insulation (Nora et al. 2017; Kubo et al. 2021). Although *CTCF* siRNA knockdown had limited effects on TAD structure, SIQHiC-normalization revealed a global decrease in chromatin contact frequency at all chromatin loop sets, demonstrating the importance of cell count normalization in analyzing the perturbation of chromatin architectural factors.

Previous research has shown that active transcription may play a role in maintaining the three-dimensional genome organization (Busslinger et al. 2017; Isoda et al. 2017; Gu et al. 2018; Heinz et al. 2018; Nagashima et al. 2019). Here, we show that transcriptional activity does correlate with chromatin interactions. Although *MYC* overexpression increases global transcription of active genes, we observed increased chromatin contact frequency regardless of transcription activity, indicating that direct binding of MYC contributes to chromatin interactions via other mechanisms.

MYC overexpression is a common event in oncogenesis across multiple cancers but cannot alone induce malignant transformation. Our results suggest that other cancer-initiating mutations are required to reconfigure the epigenetic and chromatin interaction landscape, with MYC playing a role in maintaining these epigenetic alterations by stabilizing these transient changes in chromatin interactions. These cancers would in turn become reliant on MYC and other participants of these chromatin interactions. If MYC expression is inhibited, we suspect that the reduction in protein–protein interactions will reduce these aberrant chromatin interactions.

Alternatively, these chromatin interactions can be perturbed by inhibiting other architectural factors involved. In this work, *CTCF* knockdown reduced chromatin contact frequency and dispersed MYC, supporting this line of investigation. A recent study has identified curaxins as a class of anticancer drugs that can disrupt chromatin looping by intercalating with DNA and interfering with CTCF binding (Kantidze et al. 2019), without causing DNA damage (Gasparian et al. 2011; Kantidze et al. 2019; Lu et al. 2021). Curaxins also exert anticancer activity through trapping of the histone chaperone FACT complex on chromatin (Gasparian et al. 2011). Crucially, both chromatin looping disruption and FACT complex trapping led to reduced expression of *MYC* family genes (Carter et al. 2015; Kantidze et al. 2019; Wang et al. 2020). Although complete degradation of CTCF is lethal in normal cells (Moore et al. 2012; Kemp et al. 2014), curaxins were well tolerated in xenograft models across multiple cancer cell types (Dermawan et al. 2016; Kim et al. 2016; Barone et al. 2017) and recently completed phase I clinical trials (Sarantopoulos et al. 2020), making it a promising drug against *MYC*-addicted cancers.

Taken together, our manuscript has demonstrated that *MYC* overexpression leads to MYC invasion into super-enhancers, and SIQHiC uncovered an increase in chromatin interactions at these regions. We have also shown the utility of SIQHiC in investigating chromatin architectural proteins such as CTCF. Our results lay the groundwork for further research to elucidate the role of MYC in maintaining cancer-specific chromatin interactions in established cancers and ways to therapeutically target these chromatin interactions. We anticipate that SIQHiC will continue to be useful for uncovering changes in chromatin contact frequency when perturbing chromatin architectural factors and using drugs such as curaxins.

Methods

Cell lines

U2OS osteosarcoma cells (ATCC HTB-96) with a doxycycline-inducible *MYC* system were kindly provided by Elmar Wolf's lab from Universität Würzburg, Germany. Cell lines were authenticated by STR profiling, and mycoplasma testing was performed using the MycoAlert PLUS Mycoplasma Detection kit (Lonza). U2OS cells were grown in DMEM supplemented with 10% tetracycline-free fetal bovine serum (Clontech), 100 U/mL penicillin, and 100 µg/mL streptomycin. *MYC* expression was induced in U2OS cells by the addition of 1 µg/mL doxycycline (Clontech) for 30 h. *CTCF* siRNA knockdown was performed using ON-TARGETplus SMARTpool Human CTCF (10664) siRNA (Dharmacon L-020165-00-0005). Cells were transfected with 5 nM *CTCF* siRNA using Lipofectamine RNAiMAX (Thermo Fisher

Scientific) according to the manufacturer's instructions, with medium replacement after 24 h, and cells were harvested after 48 h.

Protein extraction and Western blot

Cells were lysed in RIPA Lysis and Extraction Buffer (Thermo Fisher Scientific) for 30 min at 4°C, with vortexing every 10 min. Cell lysate was centrifuged to remove cell debris. Protein concentration was measured using the Pierce BCA Protein Assay kit (Thermo Fisher Scientific). Fifty micrograms of protein was loaded into a 12% SDS-PAGE gel for electrophoresis and transferred onto a PVDF membrane. The membrane was blocked with 5% nonfat milk in Tris- buffered saline with 0.1% Tween 20 (TBST) for 1 h at room temperature, followed by incubation with primary antibodies overnight at 4°C. The following primary antibodies were used: anti-MYC (Abcam ab32072; diluted 1:1000) and anti-vinculin (Sigma-Aldrich V9131; diluted 1:200). The membrane was washed three times with TBST, followed by incubation with either mouse (Cell Signalling Technologies 7076; diluted 1:5000) or rabbit (Cell Signalling Technologies 7074; diluted 1:5000) HRP-conjugated secondary antibodies for 1 h at room temperature. After washing three times with TBST, bands were imaged using Clarity Western ECL Substrate (Bio-Rad) on the ImageQuant LAS 500 (GE Healthcare).

Immunofluorescence staining

Cells were grown on a coverslip, fixed in 4% formaldehyde for 15 min, and permeabilized with 0.2% Triton X-100 in Tris-buffered saline (TBS-TX100). Cells were then blocked with 1% bovine serum albumin (BSA) in 0.2% TBS-TX100 for 3 h at room temperature and incubated with primary antibodies against MYC (Abcam ab32072) or RNA polymerase II (BioLegend 664906) for 2 h at room temperature. Coverslips were washed three times with 0.2% TBS-TX100, incubated with antimouse secondary antibodies conjugated with Alexa Fluor 555 (Life Technologies A21422) or antirabbit secondary antibodies conjugated with Alexa Fluor 488 (Life Technologies A11034) for 1 h at room temperature, followed by incubation with DAPI (Sigma-Aldrich) for 10 min. Coverslips were mounted onto slides and imaged on the Nikon A1R confocal microscope at 100× magnification.

Reverse transcription and quantitative polymerase chain reaction (RT-qPCR)

RNA was extracted from U2OS cells with or without *MYC* induction in triplicate, using the RNeasy Mini kit (QIAGEN). RNA was reverse-transcribed into complementary DNA using the qScript cDNA Synthesis kit (Quantabio). Quantitative PCR was performed on the QuantStudio 5 (Thermo Fisher Scientific) using the GoTaq qPCR Mastermix (Promega), with *TBP* as the housekeeping control. Primer sequences are listed in Supplemental Table S5.

Circular chromosome conformation capture experimental procedure

4C-seq was performed in duplicate on U2OS cells with or without *MYC* induction as previously described (Cao et al. 2017). Forty million cells were crosslinked in PBS supplemented with 1% formaldehyde for 10 min at room temperature, followed by quenching with 0.25 M glycine for 5 min. Cells were washed three times with PBS supplemented with 1 mM phenylmethylsulfonyl fluoride (Sigma-Aldrich). Nuclei were isolated by lysing cells in 4C lysis buffer (10 mM Tris-HCl, pH 8.0, 10 mM NaCl, 5 mM EDTA, 0.5% Igepal CA-630) for 10 min at 4°C, followed by homogenization using a dounce homogenizer (Wheaton) (50 strokes using Pestle B).

Nuclei were permeabilized at 37°C with the addition of 0.3% SDS for 1 h, followed by 2% Triton-X 100 for 1 h. Primary enzyme digestion with HindIII-HF (NEB) was done for 18 h at 37°C, before proximity ligation in dilute conditions with T4 DNA Ligase (Thermo Fisher Scientific) overnight at 16°C. Crosslinking was reversed with the addition of 55 µg/mL Proteinase K (Ambion) for 4 h at 65°C and overnight at 37°C, and treated with RNase A for 1 h at 37°C. DNA was purified using phenol/chloroform extraction followed by ethanol precipitation to yield the 3C library. Secondary enzyme digestion with DpnII (NEB) was done on the 3C library overnight at 37°C, followed by proximity ligation and de-crosslinking as described above. 4C libraries were generated for each viewpoint through nested inverse-PCR using Phusion DNA Polymerase (Thermo Fisher Scientific), with primers listed in Supplemental Table S5. DNA fragments between 200 and 1000 bp were isolated from the 4C libraries by gel excision after running the 4C libraries on a 4%–20% gradient TBE gel (Thermo Fisher Scientific). The gel slices were shredded and macerated in Tris EDTA buffer overnight at 37°C, and DNA was precipitated using ethanol. The 4C libraries were multiplexed and single-end 1 × 150-bp sequencing was performed on the Illumina MiSeq.

RNA-seq experimental procedure

Total RNA was extracted from U2OS cells with or without *MYC* induction in duplicate, using the RNeasy Mini kit (QIAGEN). Ribosomal RNA depletion and library preparation were performed using the TruSeq Stranded Total RNA LT kit (Illumina) according to the manufacturer's protocol. Paired-end 2 × 100-bp sequencing was performed on the Illumina HiSeq 2500.

ChIP-seq experimental procedure

H3K27ac and MYC ChIP-seq were performed in duplicate on U2OS cells with or without *MYC* induction. Cells were fixed in 1% formaldehyde and sonicated using the truChIP Chromatin Shearing kit (Covaris) on the ME220 Focused-Ultrasonicator (Covaris) according to the manufacturer's protocol. H3K27ac and MYC-bound DNA were immunoprecipitated using anti-H3K27ac (Abcam ab4729, Lot: GR150367-1) and anti-MYC (Santa Cruz Biotechnology sc-764, Lot: H1712), with anti-IgG (Santa Cruz Biotechnology sc-2027, Lot: H2615) as the negative control. Three and one-half micrograms of each antibody was rotated with 15 µL of Dynabeads Protein G magnetic beads (Invitrogen) overnight at 4°C and washed three times with beads wash buffer (0.1% Triton X-100 in PBS) to remove unbound antibodies. Antibody-bound beads were combined with sonicated chromatin from five million cells and rotated overnight at 4°C. Beads were then washed three times with Shearing Buffer D3 (Covaris), once with high salt washing buffer (50 mM HEPES, pH 7.5, 350 mM NaCl, 1 mM EDTA, 1% Triton X-100, 0.1% sodium deoxycholate, 0.1% SDS), once with lithium chloride wash buffer (10 mM Tris, pH 8.0, 250 mM LiCl, 1 mM EDTA, 0.5% NP-40, 0.5% sodium deoxycholate), and once with Tris-EDTA buffer. Chromatin was eluted from the magnetic beads in 100 µL elution buffer (50 mM Tris, pH 8.0, 10 mM EDTA, 1% SDS) supplemented with 2 µL of 0.5 mg/mL RNase A (QIAGEN) for 2 h at 55°C. Chromatin was then de-crosslinked with the addition of 2 µL of 20 mg/mL Proteinase K (Ambion) for 4 h at 55°C and overnight at 37°C. For total input, chromatin from 500,000 cells was treated with RNase A and de-crosslinked similarly. DNA was purified using the MinElute PCR Purification kit (QIAGEN). ChIP-seq libraries

were prepared using the ThruPLEX DNA-seq kit (Rubicon) and sequenced paired-end 2 × 100 bp on the HiSeq 2500 (Illumina).

SIQHiC experimental procedure

SIQHiC was performed in duplicate on U2OS cells with or without *MYC* induction, with the addition of untreated mouse 3T3 cells. Human U2OS cells and mouse 3T3 cells were counted using the Countess II automated cell counter (Thermo Fisher Scientific) and fixed with 2% formaldehyde using the Arima Hi-C kit (Arima Genomics). One million fixed mouse 3T3 cells were added to each sample of four million fixed human U2OS cells before subsequent steps of restriction enzyme digest, biotin end filling, and ligation using the Arima-HiC kit (Arima Genomics) according to the manufacturer's protocol. Libraries were prepared using the KAPA Hyper-Prep kit (KAPA), according to the Arima-HiC kit protocol. SIQHiC libraries were sequenced paired-end 2 × 150-bp on the HiSeq 4000 (Illumina).

Genome assembly

4C-seq, ChIP-seq, RNA-seq, and SIQHiC libraries were all mapped to the hg19 human genome assembly, in line with previous published data sets on MYC enhancer invasion that were analyzed using this assembly. We do not expect significant differences when the libraries are mapped to the newer GRCh38 genome assembly because a previous analysis of TCGA data had shown significant concordance between hg19 and GRCh38 versions (Gao et al. 2019).

4C-seq data processing

4C-seq libraries were mapped to the hg19 genome using BWA-MEM (Li 2013) version 0.7.5a-r405 using default settings, and significant 4C interactions were identified using the r3Cseq pipeline ($q < 0.05$) (Thongjuea et al. 2013) on the CSI NGS portal (An et al. 2020) (https://csibioinfo.nus.edu.sg/).

ChIP-seq data processing

ChIP-seq libraries were mapped to the hg19 genome using BWA-MEM (Li 2013) version 0.7.5a-r405 using default settings. PCR duplicates were removed using SAMtools (Li et al. 2009) version 1.7, and reads falling within the ENCODE consensus blacklisted regions (The ENCODE Project Consortium 2012) were removed using BEDTools (Quinlan and Hall 2010) version 2.26.0. ChIP-seq signals were visualized using deepTools (Ramírez et al. 2014) version 3.2.1 (bamCompare --normalizeUsing RPKM --operation subtract -bs 1). BAM files of biological replicates were merged before calling ChIP-seq peaks using MACS2 (Zhang et al. 2008) version 2.1.2. H3K27ac ChIP-seq peaks within 2 kb of transcription start sites were labeled as active promoter peaks whereas the rest were labeled as enhancer peaks.

Super-enhancers were called as described previously (Cao et al. 2017). Briefly, H3K27ac enhancer peaks within 12.5 kb of each other were stitched together and ranked based on H3K27ac enrichment. The point where a line with slope 1 is tangential to the ranked H3K27ac enrichment curve was chosen as a cutoff to separate super-enhancers from typical enhancers.

To identify differential H3K27ac peaks, BAM files from all replicates and conditions were merged and a common list of H3K27ac peaks was called using MACS2. Read counts for the common list of H3K27ac peaks were obtained using Rsubread (Liao et al. 2019). Differential H3K27ac peaks were identified using DESeq2 (Love et al. 2014) version 1.24.0 ($padj < 0.01$ and $padj < 0.01$, respectively).

Motif analysis was performed to find the frequency of HOCOMOCO Human v11 Core motifs (Kulakovskiy et al. 2018) occurring at MYC binding sites using FIMO (Grant et al. 2011) with default parameters.

RNA-seq data processing

Total RNA-seq libraries were mapped to the hg19 genome and read counts for UCSC RefSeq transcripts were obtained using kallisto v0.44.0 (Bray et al. 2016). Differentially expressed transcripts were identified using sleuth v0.30.0 (Pimentel et al. 2017) ($fdr < 0.05$, $|beta| > 1$) in R (R Core Team 2021). Gene set enrichment analysis was performed using GSEA v4.1.0 (Subramanian et al. 2005). Gene Ontology (GO) functional annotation was performed using DAVID (Huang da et al. 2009).

SIQHiC data processing

SIQHiC libraries were analyzed using the Juicer (v1.5) pipeline (Durand et al. 2016) with some modifications to obtain HIC matrix files. Because SIQHiC libraries include human and mouse DNA, paired reads were separated and mapped as single reads using BWA-MEM (Li 2013) to an artificial reference genome combining hg19 human and mm10 mouse genome sequences. Human and mouse chromosomes were appended with "H" and "M", respectively, to avoid chromosome name duplication. After mapping, reads were paired together again and split into two files. Paired reads both mapping to human chromosomes were placed together as Human-Human paired reads (H-H), and paired reads both mapping to mouse chromosomes were placed together as Mouse-Mouse paired reads (M-M). Ambiguous read pairs that separately mapped to different species were discarded. H-H and M-M reads were processed using Juicer separately, filtering out duplicates, intrafragment reads, and reads with $MAPQ < 30$ to generate HIC matrix files for each species. H-H reads of biological replicates were also merged and processed in the same way to generate HIC matrix files for downstream analyses.

The ratio between human and mouse contacts for each sample was calculated. Because the mouse 3T3 cells in each sample come from the same population and were spiked into the human cells at the same ratio of 1:4, we expect to obtain a similar HMR ratio across all samples. Hence, the relative difference between the HMR of different samples (SIQHiC ratio) reflects the changes in global chromatin contact frequency. The SIQHiC ratio was calculated such that samples with lower HMR are normalized against samples with the highest HMR.

Hi-C contact matrices from merged biological replicates were normalized using the SIQHiC ratio by adding a custom normalization vector to the original contact matrix HIC file using the Juicer "addNorm" subroutine, where the magnitude of each bin was the SIQHiC ratio raised to the power of (−0.5). In this way, the Hi-C matrices are cell count-normalized to the sample with the highest HMR to prevent scale-up extrapolation errors.

The SIQHiC normalized matrix for each chromosome was extracted from the HIC file using the Juicer "dump" subroutine, combined together, and finally reassembled into a SIQHiC normalized HIC matrix file using the Juicer "pre" subroutine. Because the SIQHiC normalization vector for the High *MYC* Hi-C matrix is 1, the SIQHiC normalized matrix is equivalent to the nonnormalized matrix. Hence, only the Low *MYC* Hi-C matrix was SIQHiC-normalized. Original and SIQHiC-normalized HIC matrices were balanced using the Knight-Ruiz algorithm for subsequent analyses.

Aggregate peak analyses was performed using the Juicer "apa" subroutine using both nonnormalized and SIQHiC-normalized contact matrices using the parameters "-k KR –u –n 30". APA

heat maps were generated using pheatmap v1.0.12 (https://rdrr.io/cran/pheatmap/) in R (R Core Team 2021).

Compartments were identified using the Juicer "eigenvector" and "pearsons" subroutines at 100-kb resolution. Because eigenvalues signs are arbitrary, we correlated eigenvectors with the number of gene promoters within each 100-kb bin, such that gene rich regions were assigned positive eigenvalues.

Topologically associating domain boundaries were identified using the HiCExplorer (Ramírez et al. 2018) "hicFindTADs" subroutine using the parameter "--minDepth 50000 --maxDepth 500000 --thresholdComparisons 0.001 --delta 0.01 --correctForMultipleTesting fdr". Lost, common, and gained TAD boundaries were identified by intersecting Low *MYC* and High *MYC* TAD boundaries. TAD separation scores of lost, common, and gained TAD boundaries were visualized using deepTools (Ramírez et al. 2014) version 3.2.1.

Loops were called using the Juicer "hiccups" subroutine with parameter "-k KR -m 1024 --ignore_sparsity". Lost, common, and gained loops were identified using pgltools (Greenwald et al. 2017) by merging and intersecting Low *MYC* loops with High *MYC* loops using a 10-kb intersecting window at each loop anchor. Loop subsets are listed in Supplemental Table S5. Hi-C loops were annotated according to their overlap with MYC binding sites, promoters, typical enhancers, and super-enhancers using pgltools.

Virtual 4C tracks were extracted from the Hi-C matrices by using the Juicer "dump" subroutine, dumping a 5-kb window against its entire chromosome using a 5-kb bin size.

Data access

All raw and processed sequencing data generated in this study have been submitted to the NCBI Gene Expression Omnibus (GEO; https://www.ncbi.nlm.nih.gov/geo/) under accession number GSE164777.

Competing interest statement

M.J.F. declares two patents on methodologies related to ChIA-PET. No other competing interests are declared.

Acknowledgments

This research is supported by the RNA Biology Center at the Cancer Science Institute of Singapore, NUS, as part of funding under the Singapore Ministry of Education Academic Research Fund Tier 3 grant awarded to Daniel Tenen (MOE2014-T3-1-006). This research is supported by the NRF Singapore and the Singapore Ministry of Education under its Research Centres of Excellence initiative and a Singapore Ministry of Education Academic Research Fund Tier 2 grant awarded to M.J.F. (MOET2EP30120-0009).

Author contributions: Y.X.S. and M.J.F. contributed to the conception and design of the study. Y.X.S. conducted the experiments and developed the SIQHiC protocol. Y.X.S. and K.C. performed the bioinformatics analyses. Y.X.S. and M.J.F. reviewed the data and wrote the manuscript. All authors reviewed and approved the manuscript.

References

Affer M, Chesi M, Chen WD, Keats JJ, Demchenko YN, Tamizhmani K, Garbitt VM, Riggs DL, Brents LA, Roschke AV, et al. 2014. Promiscuous MYC locus rearrangements hijack enhancers but mostly super-enhancers to dysregulate MYC expression in multiple myeloma. *Leukemia* **28:** 1725–1735. doi:10.1038/leu.2014.70

An O, Tan KT, Li Y, Li J, Wu CS, Zhang B, Chen L, Yang H. 2020. CSI NGS Portal: an online platform for automated NGS data analysis and sharing. *Int J Mol Sci* **21:** 3828. doi:10.3390/ijms21113828

Babu D, Fullwood MJ. 2015. 3D genome organization in health and disease: emerging opportunities in cancer translational medicine. *Nucleus* **6:** 382–393. doi:10.1080/19491034.2015.1106676

Bahr C, von Paleske L, Uslu VV, Remeseiro S, Takayama N, Ng SW, Murison A, Langenfeld K, Petretich M, Scognamiglio R, et al. 2018. A *Myc* enhancer cluster regulates normal and leukaemic haematopoietic stem cell hierarchies. *Nature* **553:** 515–520. doi:10.1038/nature25193

Barone TA, Burkhart CA, Safina A, Haderski G, Gurova KV, Purmal AA, Gudkov AV, Plunkett RJ. 2017. Anticancer drug candidate CBL0137, which inhibits histone chaperone FACT, is efficacious in preclinical orthotopic models of temozolomide-responsive and -resistant glioblastoma. *Neuro Oncol* **19:** 186–196. doi:10.1093/neuonc/now141

Beagrie RA, Scialdone A, Schueler M, Kraemer DC, Chotalia M, Xie SQ, Barbieri M, de Santiago I, Lavitas LM, Branco MR, et al. 2017. Complex multi-enhancer contacts captured by genome architecture mapping. *Nature* **543:** 519–524. doi:10.1038/nature21411

Beroukhim R, Mermel CH, Porter D, Wei G, Raychaudhuri S, Donovan J, Barretina J, Boehm JS, Dobson J, Urashima M, et al. 2010. The landscape of somatic copy-number alteration across human cancers. *Nature* **463:** 899–905. doi:10.1038/nature08822

Bradner JE, Hnisz D, Young RA. 2017. Transcriptional addiction in cancer. *Cell* **168:** 629–643. doi:10.1016/j.cell.2016.12.013

Bray NL, Pimentel H, Melsted P, Pachter L. 2016. Near-optimal probabilistic RNA-seq quantification. *Nat Biotechnol* **34:** 525–527. doi:10.1038/nbt.3519

Busslinger GA, Stocsits RR, van der Lelij P, Axelsson E, Tedeschi A, Galjart N, Peters JM. 2017. Cohesin is positioned in mammalian genomes by transcription, CTCF and Wapl. *Nature* **544:** 503–507. doi:10.1038/nature22063

Cao F, Fang Y, Tan HK, Goh Y, Choy JYH, Koh BTH, Tan JH, Bertin N, Ramadass A, Hunter E, et al. 2017. Super-enhancers and broad H3K4me3 domains form complex gene regulatory circuits involving chromatin interactions. *Sci Rep* **7:** 2186. doi:10.1038/s41598-017-02257-3

Carter D, Chakalova L, Osborne CS, Dai YF, Fraser P. 2002. Long-range chromatin regulatory interactions *in vivo*. *Nat Genet* **32:** 623–626. doi:10.1038/ng1051

Carter DR, Murray J, Cheung BB, Gamble L, Koach J, Tsang J, Sutton S, Kalla H, Syed S, Gifford AJ, et al. 2015. Therapeutic targeting of the MYC signal by inhibition of histone chaperone FACT in neuroblastoma. *Sci Transl Med* **7:** 312ra176. doi:10.1126/scitranslmed.aab1803

de Pretis S, Kress TR, Morelli MJ, Sabò A, Locarno C, Verrecchia A, Doni M, Campaner S, Amati B, Pelizzola M. 2017. Integrative analysis of RNA polymerase II and transcriptional dynamics upon MYC activation. *Genome Res* **27:** 1658–1664. doi:10.1101/gr.226035.117

Dermawan JKT, Hitomi M, Silver DJ, Wu Q, Sandlesh P, Sloan AE, Purmal AA, Gurova KV, Rich JN, Lathia JD, et al. 2016. Pharmacological targeting of the histone chaperone complex FACT preferentially eliminates glioblastoma stem cells and prolongs survival in preclinical models. *Cancer Res* **76:** 2432–2442. doi:10.1158/0008-5472.CAN-15-2162

Durand NC, Shamim MS, Machol I, Rao SSP, Huntley MH, Lander ES, Aiden EL. 2016. Juicer provides a one-click system for analyzing loop-resolution Hi-C experiments. *Cell Syst* **3:** 95–98. doi:10.1016/j.cels.2016.07.002

Eilers M, Eisenman RN. 2008. Myc's broad reach. *Genes Dev* **22:** 2755–2766. doi:10.1101/gad.1712408

The ENCODE Project Consortium. 2012. An integrated encyclopedia of DNA elements in the human genome. *Nature* **489:** 57–74. doi:10.1038/nature11247

Gabay M, Li Y, Felsher DW. 2014. MYC activation is a hallmark of cancer initiation and maintenance. *Cold Spring Harb Perspect Med* **4:** a014241. doi:10.1101/cshperspect.a014241

Gao GF, Parker JS, Reynolds SM, Silva TC, Wang L-B, Zhou W, Akbani R, Bailey M, Balu S, Berman BP, et al. 2019. Before and after: comparison of legacy and harmonized TCGA Genomic Data Commons' data. *Cell Syst* **9:** 24–34.e10. doi:10.1016/j.cels.2019.06.006

Gasparian AV, Burkhart CA, Purmal AA, Brodsky L, Pal M, Saranadasa M, Bosykh DA, Commane M, Guryanova OA, Pal S, et al. 2011. Curaxins: anticancer compounds that simultaneously suppress NF-κB and activate p53 by targeting FACT. *Sci Transl Med* **3:** 95ra74. doi:10.1126/scitranslmed.3002530

Grant CE, Bailey TL, Noble WS. 2011. FIMO: scanning for occurrences of a given motif. *Bioinformatics* **27:** 1017–1018. doi:10.1093/bioinformatics/btr064

Greenwald WW, Li H, Smith EN, Benaglio P, Nariai N, Frazer KA. 2017. Pgltools: a genomic arithmetic tool suite for manipulation of Hi-C peak and other chromatin interaction data. *BMC Bioinformatics* **18:** 207. doi:10.1186/s12859-017-1621-0

Gryder BE, Pomella S, Sayers C, Wu XS, Song Y, Chiarella AM, Bagchi S, Chou H-C, Sinniah RS, Walton A, et al. 2019. Histone hyperacetylation disrupts core gene regulatory architecture in rhabdomyosarcoma. *Nat Genet* **51:** 1714–1722. doi:10.1038/s41588-019-0534-4

Gu B, Swigut T, Spencley A, Bauer MR, Chung M, Meyer T, Wysocka J. 2018. Transcription-coupled changes in nuclear mobility of mammalian *cis*-regulatory elements. *Science* **359:** 1050–1055. doi:10.1126/science.aao3136

Guccione E, Martinato F, Finocchiaro G, Luzi L, Tizzoni L, Dall' Olio V, Zardo G, Nervi C, Bernard L, Amati B. 2006. Myc-binding-site recognition in the human genome is determined by chromatin context. *Nat Cell Biol* **8:** 764–770. doi:10.1038/ncb1434

Heinz S, Texari L, Hayes MGB, Urbanowski M, Chang MW, Givarkes N, Rialdi A, White KM, Albrecht RA, Pache L, et al. 2018. Transcription elongation can affect genome 3D structure. *Cell* **174:** 1522–1536.e22. doi:10.1016/j.cell.2018.07.047

Herranz D, Ambesi-Impiombato A, Palomero T, Schnell SA, Belver L, Wendorff AA, Xu L, Castillo-Martin M, Llobet-Navás D, Cordon-Cardo C, et al. 2014. A NOTCH1-driven *MYC* enhancer promotes T cell development, transformation and acute lymphoblastic leukemia. *Nat Med* **20:** 1130–1137. doi:10.1038/nm.3665

Hnisz D, Abraham BJ, Lee TI, Lau A, Saint-André V, Sigova AA, Hoke HA, Young RA. 2013. Super-enhancers in the control of cell identity and disease. *Cell* **155:** 934–947. doi:10.1016/j.cell.2013.09.053

Huang da W, Sherman BT, Lempicki RA. 2009. Systematic and integrative analysis of large gene lists using DAVID bioinformatics resources. *Nat Protoc* **4:** 44–57. doi:10.1038/nprot.2008.211

Hyle J, Zhang Y, Wright S, Xu B, Shao Y, Easton J, Tian L, Feng R, Xu P, Li C. 2019. Acute depletion of CTCF directly affects *MYC* regulation through loss of enhancer–promoter looping. *Nucleic Acids Res* **47:** 6699–6713. doi:10.1093/nar/gkz462

Isoda T, Moore AJ, He Z, Chandra V, Aida M, Denholtz M, Piet van Hamburg J, Fisch KM, Chang AN, Fahl SP, et al. 2017. Non-coding transcription instructs chromatin folding and compartmentalization to dictate enhancer-promoter communication and T cell fate. *Cell* **171:** 103–119.e18. doi:10.1016/j.cell.2017.09.001

Kantidze OL, Luzhin AV, Nizovtseva EV, Safina A, Valieva ME, Golov AK, Velichko AK, Lyubitelev AV, Feofanov AV, Gurova KV, et al. 2019. The anti-cancer drugs curaxins target spatial genome organization. *Nat Commun* **10:** 1441. doi:10.1038/s41467-019-09500-7

Kemp CJ, Moore JM, Moser R, Bernard B, Teater M, Smith LE, Rabaia NA, Gurley KE, Guinney J, Busch SE, et al. 2014. CTCF haploinsufficiency destabilizes DNA methylation and predisposes to cancer. *Cell Rep* **7:** 1020–1029. doi:10.1016/j.celrep.2014.04.004

Khoury A, Achinger-Kawecka J, Bert SA, Smith GC, French HJ, Luu P-L, Peters TJ, Du Q, Parry AJ, Valdes-Mora F, et al. 2020. Constitutively bound CTCF sites maintain 3D chromatin architecture and long-range epigenetically regulated domains. *Nat Commun* **11:** 54. doi:10.1038/s41467-019-13753-7

Kieffer-Kwon K-R, Nimura K, Rao SSP, Xu J, Jung S, Pekowska A, Dose M, Stevens E, Mathe E, Dong P, et al. 2017. Myc regulates chromatin decompaction and nuclear architecture during B cell activation. *Mol Cell* **67:** 566–578.e10. doi:10.1016/j.molcel.2017.07.013

Kim M, Neznanov N, Wilfong CD, Fleyshman DI, Purmal AA, Haderski G, Stanhope-Baker P, Burkhart CA, Gurova KV, Gudkov AV, et al. 2016. Preclinical validation of a single-treatment infusion modality that can eradicate extremity melanomas. *Cancer Res* **76:** 6620–6630. doi:10.1158/0008-5472.CAN-15-2764

Kress TR, Sabò A, Amati B. 2015. MYC: connecting selective transcriptional control to global RNA production. *Nat Rev Cancer* **15:** 593–607. doi:10.1038/nrc3984

Kubo N, Ishii H, Xiong X, Bianco S, Meitinger F, Hu R, Hocker JD, Conte M, Gorkin D, Yu M, et al. 2021. Promoter-proximal CTCF binding promotes distal enhancer-dependent gene activation. *Nat Struct Mol Biol* **28:** 152–161. doi:10.1038/s41594-020-00539-5

Kulakovskiy IV, Vorontsov IE, Yevshin IS, Sharipov RN, Fedorova AD, Rumynskiy EI, Medvedeva YA, Magana-Mora A, Bajic VB, Papatsenko DA, et al. 2018. HOCOMOCO: towards a complete collection of transcription factor binding models for human and mouse via large-scale ChIP-Seq analysis. *Nucleic Acids Res* **46:** D252–D259. doi:10.1093/nar/gkx1106

Li H. 2013. Aligning sequence reads, clone sequences and assembly contigs with BWA-MEM. arXiv:1303.3997 [q-bio.GN].

Li H, Handsaker B, Wysoker A, Fennell T, Ruan J, Homer N, Marth G, Abecasis G, Durbin R, 1000 Genome Project Data Processing Consortium. 2009. The Sequence Alignment/Map format and SAMtools. *Bioinformatics* **25:** 2078–2079. doi:10.1093/bioinformatics/btp352

Liao Y, Smyth GK, Shi W. 2019. The R package *Rsubread* is easier, faster, cheaper and better for alignment and quantification of RNA sequencing reads. *Nucleic Acids Res* **47:** e47. doi:10.1093/nar/gkz114

Lin CY, Lovén J, Rahl PB, Paranal RM, Burge CB, Bradner JE, Lee TI, Young RA. 2012. Transcriptional amplification in tumor cells with elevated c-Myc. *Cell* **151:** 56–67. doi:10.1016/j.cell.2012.08.026

Lorenzin F, Benary U, Baluapuri A, Walz S, Jung LA, von Eyss B, Kisker C, Wolf J, Eilers M, Wolf E. 2016. Different promoter affinities account for specificity in MYC-dependent gene regulation. *eLife* **5:** e15161. doi:10.7554/eLife.15161

Love MI, Huber W, Anders S. 2014. Moderated estimation of fold change and dispersion for RNA-seq data with DESeq2. *Genome Biol* **15:** 550. doi:10.1186/s13059-014-0550-8

Lovén J, Orlando DA, Sigova AA, Lin CY, Rahl PB, Burge CB, Levens DL, Lee TI, Young RA. 2012. Revisiting global gene expression analysis. *Cell* **151:** 476–482. doi:10.1016/j.cell.2012.10.012

Lovén J, Hoke HA, Lin CY, Lau A, Orlando DA, Vakoc CR, Bradner JE, Lee TI, Young RA. 2013. Selective inhibition of tumor oncogenes by disruption of super-enhancers. *Cell* **153:** 320–334. doi:10.1016/j.cell.2013.03.036

Lu K, Liu C, Liu Y, Luo A, Chen J, Lei Z, Kong J, Xiao X, Zhang S, Wang Y-Z, et al. 2021. Curaxin-induced DNA topology alterations trigger the distinct binding response of CTCF and FACT at the single-molecule level. *Biochemistry* **60:** 494–499. doi:10.1021/acs.biochem.1c00014

Lun ATL, Smyth GK. 2015. diffHic: a Bioconductor package to detect differential genomic interactions in Hi-C data. *BMC Bioinformatics* **16:** 258. doi:10.1186/s12859-015-0683-0

McKeown MR, Bradner JE. 2014. Therapeutic strategies to inhibit MYC. *Cold Spring Harb Perspect Med* **4:** a014266. doi:10.1101/cshperspect.a014266

Moore JM, Rabaia NA, Smith LE, Fagerlie S, Gurley K, Loukinov D, Disteche CM, Collins SJ, Kemp CJ, Lobanenkov VV, et al. 2012. Loss of maternal CTCF is associated with peri-implantation lethality of *Ctcf* null embryos. *PLoS One* **7:** e34915. doi:10.1371/journal.pone.0034915

Nagashima R, Hibino K, Ashwin SS, Babokhov M, Fujishiro S, Imai R, Nozaki T, Tamura S, Tani T, Kimura H, et al. 2019. Single nucleosome imaging reveals loose genome chromatin networks via active RNA polymerase II. *J Cell Biol* **218:** 1511–1530. doi:10.1083/jcb.201811090

Nie Z, Hu G, Wei G, Cui K, Yamane A, Resch W, Wang R, Green DR, Tessarollo L, Casellas R, et al. 2012. c-Myc is a universal amplifier of expressed genes in lymphocytes and embryonic stem cells. *Cell* **151:** 68–79. doi:10.1016/j.cell.2012.08.033

Nie Z, Guo C, Das SK, Chow CC, Batchelor E, Simons SSJ, Levens D. 2020. Dissecting transcriptional amplification by MYC. *eLife* **9:** e52483. doi:10.7554/eLife.52483

Nora EP, Goloborodko A, Valton AL, Gibcus JH, Uebersohn A, Abdennur N, Dekker J, Mirny LA, Bruneau BG. 2017. Targeted degradation of CTCF decouples local insulation of chromosome domains from genomic compartmentalization. *Cell* **169:** 930–944.e22. doi:10.1016/j.cell.2017.05.004

Ooi WF, Xing M, Xu C, Yao X, Ramlee MK, Lim MC, Cao F, Lim K, Babu D, Poon L-F, et al. 2016. Epigenomic profiling of primary gastric adenocarcinoma reveals super-enhancer heterogeneity. *Nat Commun* **7:** 12983. doi:10.1038/ncomms12983

Orlando DA, Chen MW, Brown VE, Solanki S, Choi YJ, Olson ER, Fritz CC, Bradner JE, Guenther MG. 2014. Quantitative ChIP-Seq normalization reveals global modulation of the epigenome. *Cell Rep* **9:** 1163–1170. doi:10.1016/j.celrep.2014.10.018

Pachano T, Sánchez-Gaya V, Ealo T, Mariner-Faulí M, Bleckwehl T, Asenjo HG, Respuela P, Cruz-Molina S, Muñoz-San Martín M, Haro E, et al. 2021. Orphan CpG islands amplify poised enhancer regulatory activity and determine target gene responsiveness. *Nat Genet* **53:** 1036–1049. doi:10.1038/s41588-021-00888-x

Pimentel H, Bray NL, Puente S, Melsted P, Pachter L. 2017. Differential analysis of RNA-seq incorporating quantification uncertainty. *Nat Methods* **14:** 687–690. doi:10.1038/nmeth.4324

Plank JL, Dean A. 2014. Enhancer function: mechanistic and genome-wide insights come together. *Mol Cell* **55:** 5–14. doi:10.1016/j.molcel.2014.06.015

Poli V, Fagnocchi L, Fasciani A, Cherubini A, Mazzoleni S, Ferrillo S, Miluzio A, Gaudioso G, Vaira V, Turdo A, et al. 2018. MYC-driven epigenetic reprogramming favors the onset of tumorigenesis by inducing a stem cell-like state. *Nat Commun* **9:** 1024. doi:10.1038/s41467-018-03264-2

Quinlan AR, Hall IM. 2010. BEDTools: a flexible suite of utilities for comparing genomic features. *Bioinformatics* **26:** 841–842. doi:10.1093/bioinformatics/btq033

Raisner R, Bainer R, Haverty PM, Benedetti KL, Gascoigne KE. 2020. Super-enhancer acquisition drives oncogene expression in triple negative breast cancer. *PLoS One* **15:** e0235343. doi:10.1371/journal.pone.0235343

Ramírez F, Dündar F, Diehl S, Grüning BA, Manke T. 2014. deepTools: a flexible platform for exploring deep-sequencing data. *Nucleic Acids Res* **42:** W187–W191. doi:10.1093/nar/gku365

Ramírez F, Bhardwaj V, Arrigoni L, Lam KC, Grüning BA, Villaveces J, Habermann B, Akhtar A, Manke T. 2018. High-resolution TADs reveal

DNA sequences underlying genome organization in flies. *Nat Commun* **9:** 189. doi:10.1038/s41467-017-02525-w

R Core Team. 2021. *R: a language and environment for statistical computing*. R Foundation for Statistical Computing, Vienna. https://www.R-project.org/.

Rodríguez-Carballo E, Gámez B, Ventura F. 2016. P38 MAPK signaling in osteoblast differentiation. *Front Cell Dev Biol* **4:** 40. doi:10.3389/fcell.2016.00040

Sabò A, Kress TR, Pelizzola M, de Pretis S, Gorski MM, Tesi A, Morelli MJ, Bora P, Doni M, Verrecchia A, et al. 2014. Selective transcriptional regulation by Myc in cellular growth control and lymphomagenesis. *Nature* **511:** 488–492. doi:10.1038/nature13537

Sarantopoulos J, Mahalingam D, Sharma N, Iyer RV, Ma WW, Ahluwalia MS, Johnson S, Purmal A, Shpigotskaya P, Hards A, et al. 2020. Results of a completed phase I trial of CBL0137 administered intravenously (IV) to patients (Pts) with advanced solid tumors. *J Clin Oncol* **38:** 3583. doi:10.1200/JCO.2020.38.15_suppl.3583

Sati S, Cavalli G. 2017. Chromosome conformation capture technologies and their impact in understanding genome function. *Chromosoma* **126:** 33–44. doi:10.1007/s00412-016-0593-6

Schaub FX, Dhankani V, Berger AC, Trivedi M, Richardson AB, Shaw R, Zhao W, Zhang X, Ventura A, Liu Y, et al. 2018. Pan-cancer alterations of the MYC oncogene and its proximal network across the Cancer Genome Atlas. *Cell Syst* **6:** 282–300.e2. doi:10.1016/j.cels.2018.03.003

Schmitt AD, Hu M, Jung I, Xu Z, Qiu Y, Tan CL, Li Y, Lin S, Lin Y, Barr CL, et al. 2016. A compendium of chromatin contact maps reveals spatially active regions in the human genome. *Cell Rep* **17:** 2042–2059. doi:10.1016/j.celrep.2016.10.061

Shi J, Whyte WA, Zepeda-Mendoza CJ, Milazzo JP, Shen C, Roe J-S, Minder JL, Mercan F, Wang E, Eckersley-Maslin MA, et al. 2013. Role of SWI/SNF in acute leukemia maintenance and enhancer-mediated *Myc* regulation. *Genes Dev* **27:** 2648–2662. doi:10.1101/gad.232710.113

Soufi A, Donahue G, Zaret KS. 2012. Facilitators and impediments of the pluripotency reprogramming factors' initial engagement with the genome. *Cell* **151:** 994–1004. doi:10.1016/j.cell.2012.09.045

Stansfield JC, Cresswell KG, Vladimirov VI, Dozmorov MG. 2018. HiCcompare: an R-package for joint normalization and comparison of HI-C datasets. *BMC Bioinformatics* **19:** 279. doi:10.1186/s12859-018-2288-x

Subramanian A, Tamayo P, Mootha VK, Mukherjee S, Ebert BL, Gillette MA, Paulovich A, Pomeroy SL, Golub TR, Lander ES, et al. 2005. Gene set enrichment analysis: a knowledge-based approach for interpreting genome-wide expression profiles. *Proc Natl Acad Sci* **102:** 15545–15550. doi:10.1073/pnas.0506580102

Thongjuea S, Stadhouders R, Grosveld FG, Soler E, Lenhard B. 2013. r3Cseq: an R/Bioconductor package for the discovery of long-range genomic interactions from chromosome conformation capture and next-generation sequencing data. *Nucleic Acids Res* **41:** e132. doi:10.1093/nar/gkt373

Tsang FH, Law CT, Tang TC, Cheng CL, Chin DW, Tam WV, Wei L, Wong CC, Ng IO, Wong CM. 2019. Aberrant super-enhancer landscape in human hepatocellular carcinoma. *Hepatology (Baltimore, Md)* **69:** 2502–2517. doi:10.1002/hep.30544

Walz S, Lorenzin F, Morton J, Wiese KE, von Eyss B, Herold S, Rycak L, Dumay-Odelot H, Karim S, Bartkuhn M, et al. 2014. Activation and repression by oncogenic MYC shape tumour-specific gene expression profiles. *Nature* **511:** 483–487. doi:10.1038/nature13473

Wang J, Sui Y, Li Q, Zhao Y, Dong X, Yang J, Liang Z, Han Y, Tang Y, Ma J. 2020. Effective inhibition of MYC-amplified group 3 medulloblastoma by FACT-targeted curaxin drug CBL0137. *Cell Death Dis* **11:** 1029. doi:10.1038/s41419-020-03201-6

Whyte WA, Orlando DA, Hnisz D, Abraham BJ, Lin CY, Kagey MH, Rahl PB, Lee TI, Young RA. 2013. Master transcription factors and mediator establish super-enhancers at key cell identity genes. *Cell* **153:** 307–319. doi:10.1016/j.cell.2013.03.035

Zeid R, Lawlor MA, Poon E, Reyes JM, Fulciniti M, Lopez MA, Scott TG, Nabet B, Erb MA, Winter GE, et al. 2018. Enhancer invasion shapes MYCN-dependent transcriptional amplification in neuroblastoma. *Nat Genet* **50:** 515–523. doi:10.1038/s41588-018-0044-9

Zhang Y, Liu T, Meyer CA, Eeckhoute J, Johnson DS, Bernstein BE, Nusbaum C, Myers RM, Brown M, Li W, et al. 2008. Model-based Analysis of ChIP-Seq (MACS). *Genome Biol* **9:** R137. doi:10.1186/gb-2008-9-9-r137

Zhang X, Choi PS, Francis JM, Imielinski M, Watanabe H, Cherniack AD, Meyerson M. 2016. Identification of focally amplified lineage-specific super-enhancers in human epithelial cancers. *Nat Genet* **48:** 176–182. doi:10.1038/ng.3470

Zuin J, Dixon JR, van der Reijden MIJA, Ye Z, Kolovos P, Brouwer RWW, van de Corput MPC, van de Werken HJG, Knoch TA, van Ijcken WFJ, et al. 2014. Cohesin and CTCF differentially affect chromatin architecture and gene expression in human cells. *Proc Natl Acad Sci* **111:** 996–1001. doi:10.1073/pnas.1317788111

Received October 21, 2021; accepted in revised form January 28, 2022.